

## Magnetic Focusing of Composite Fermions through Arrays of Cavities

J. H. Smet, D. Weiss, R. H. Blick, G. Lütjering, and K. von Klitzing

*Max-Planck Institut für Festkörperforschung, Heisenbergstrasse 1, D-70569 Stuttgart, Germany*

R. Fleischmann, R. Ketzmerick, and T. Geisel

*Institut für Theoretische Physik und SFB Nichtlineare Dynamik, Universität Frankfurt, D-60054 Frankfurt/Main, Germany*

G. Weimann

*Fraunhofer Institut für Angewandte Festkörperphysik, D-79108 Freiburg, Germany*

(Received 9 February 1996)

The magnetoresistance  $R_{xx}$  was investigated in arrays of abutted square cavities with lengths  $L$  ranging from 500 nm to 1.2  $\mu\text{m}$  near filling factor  $\nu = 1/2$ . Maxima in  $R_{xx}$  occur for effective magnetic field values satisfying the magnetic focusing condition between the cavity spacing and the cyclotron radius of composite fermions, also for the effective magnetic field direction when composite fermions are deflected in the direction *opposite* to that of electrons. The experimental data are compared with simulation results based on a quasiclassical dynamics of composite fermions in soft potentials. [S0031-9007(96)01048-4]

PACS numbers: 73.40.Hm, 05.45.+b, 73.50.Jt

Although the physical mechanisms responsible for the integer quantum Hall effect (IQHE), accounted for in a single electron picture, and the fractional quantum Hall effect (FQHE), where electron-electron interaction effects play a decisive role, are quite different, there exists a striking similarity in experiment. The latter has motivated Jain [1] to put forward the composite fermion (CF) picture in which the electron-electron interaction manifests itself in a nucleation of an even number of flux quanta to each electron resulting in CFs experiencing a reduced external magnetic field. The FQHE may then be regarded as the IQHE of CFs on an effective magnetic field scale  $B_{\text{eff}}$ , where  $B_{\text{eff}}$  is zero at filling factor  $\nu = 1/2$ , positive for  $\nu < 1/2$ , and negative for  $\nu > 1/2$ . Furthermore, Halperin *et al.* [2] have predicted the existence of a Fermi sea and a well-defined Fermi wave vector for CFs, pointing the way towards quasiclassical experiments, such as commensurability oscillations in periodic structures and transverse magnetic focusing, to prove the existence of these quasiparticles and their quasiclassical cyclotron motion. Surprisingly, such “classical” size effects were found in antidot-array [3], surface-acoustic-wave [4], and magnetic-focusing experiments [5]. However, the latter experiment fails to show focusing for  $B_{\text{eff}} < 0$  upon collector-injector reversal when CFs are supposed to deflect opposite to the direction of electrons. Here, magnetic focusing is investigated in a different geometry. Arrays of micron-sized cavities (Fig. 1), originally designed for studying interference phenomena [6], were chosen, because they exhibit large electron-focusing peaks similar to a device explored by Nakamura *et al.* [7] and allow for ensemble averaging in a single measurement to effectively suppress conductance fluctuations [8]. For sufficiently small cavities, clear CF focusing signals can be discerned also for negative  $B_{\text{eff}}$  (contrary to pre-

vious findings). Another central difference to the experiments of Goldman *et al.* [5] is the absence of focusing for increased cavity spacing  $L$ . These and other observed experimental features are in remarkable agreement with quasiclassical calculations of the CF dynamics in soft potentials.

The samples were prepared from a high-mobility GaAs-AlGaAs heterojunction. Under brief illumination with a red light-emitting diode (LED), the carrier density  $n_s$  and electron mobility  $\mu$  at 1.5 K, prior to electron-beam lithography, were, respectively,  $\approx 1.9 \times 10^{11} \text{ cm}^{-2}$  and  $2.4 \times 10^6 \text{ cm}^2/\text{V s}$ , corresponding to an elastic mean free

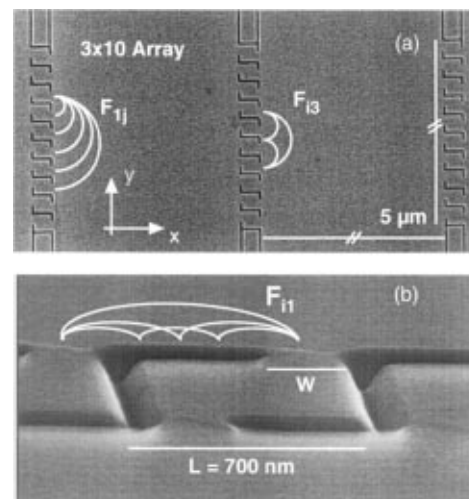


FIG. 1. (a) Scanning electron micrograph of a  $3 \times 10$  square cavity array with a period  $L$  of 500 nm and a row distance of  $5 \mu\text{m}$  and (b) an enlargement under an angle of  $75^\circ$  of a 700 nm cavity with a lithographic opening width  $W$  of 230 nm. Transverse magnetic-focusing trajectories  $F_{ij}$  for harmonic index  $i$  and subharmonic index  $j$  have been added.

path,  $L_f^e$ , of  $\approx 17.3 \mu\text{m}$ . The longitudinal resistivity at filling factor  $\nu = 1/2$ ,  $\rho_{xx}^{\text{CF}}$ , is approximately 50 times the zero-field resistivity,  $\rho_{xx}^e$ , from which one estimates a CF mean free path,  $L_f^{\text{CF}} = (\sqrt{2} \rho_{xx}^e / \rho_{xx}^{\text{CF}}) L_f^e$ , of 500 nm. Hall bars with alloyed AuGe/Ni/Au contact pads were fabricated by standard techniques. Arrays of square cavities, with lengths ranging from 500 nm to  $1.2 \mu\text{m}$  and consisting of 3 rows (in series) of 10 cavities (in parallel), were defined by electron-beam lithography (Fig. 1) and a subsequent reactive ion etch with  $\text{SiCl}_4$ . The cavities have an opening width  $W$  of  $\approx 230 \text{ nm}$ . Four-point magnetoresistance measurements, sketched in the inset of Fig. 2, were carried out in a dilution refrigerator with an 18 T superconducting coil using standard ac lock-in techniques with the external magnetic field applied perpendicular to the two-dimensional electron gas. In the dark the cavity openings were depleted and carriers appeared only after brief illumination with a red LED. Magnetoresistance traces of the 500 nm period cavity array and an adjacent unpatterned reference section of the Hall bar for magnetic fields up to 18 T are presented in Fig. 2. The magnetic field position  $B_{1/2}$  at half filling was determined from nearby well-developed fractions with an uncertainty of  $\pm 50 \text{ mT}$ .

Figure 3 shows expanded views of the magnetoresistance  $R_{xx}$  near  $B = 0$  of the  $L = 500 \text{ nm}$ ,  $700 \text{ nm}$ , and  $1.2 \mu\text{m}$  cavity arrays. The sharp features in  $R_{xx}$  occur for magnetic fields satisfying the following matching condition between the center-to-center spacing  $L$  of adjacent constrictions and the electron cyclotron radius  $R_c^e$  [9],

$$2R_c^e i = Lj \quad \text{with } i, j = 1, 2, \dots, \quad (1)$$

for which electrons transmitted through one of the cavity openings is focused into another cavity, resulting in a resistance maximum. The electron trajectories  $F_{ij}$  for different harmonic index  $i$  and subharmonic index  $j$  are illustrated in Fig. 1. When the cyclotron diameter becomes comparable to the effective width of the cavity openings, the resolution of the collecting constriction to

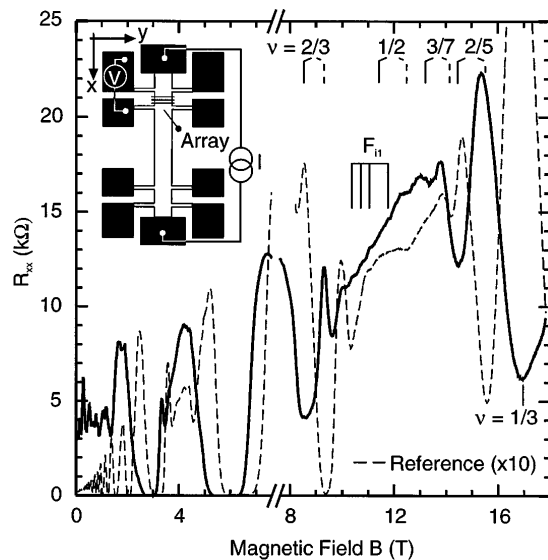


FIG. 2. Comparison of the magnetoresistance  $R_{xx} = V/I$  of an  $L = 500 \text{ nm}$  cavity array (solid) with that of the adjacent unpatterned reference section (dashed) of the Hall bar with a carrier concentration of  $1.5 \times 10^{11} \text{ cm}^{-2}$ —after weak illumination—for magnetic fields up to 18 T at 180 mK. The solid trace between 10 and 12 T is blown up in Fig. 3(a). The cool down procedure (for a description see Ref. [14]), used to minimize  $\rho_{xx}^{\text{CF}}$ , accounts for the axis break.

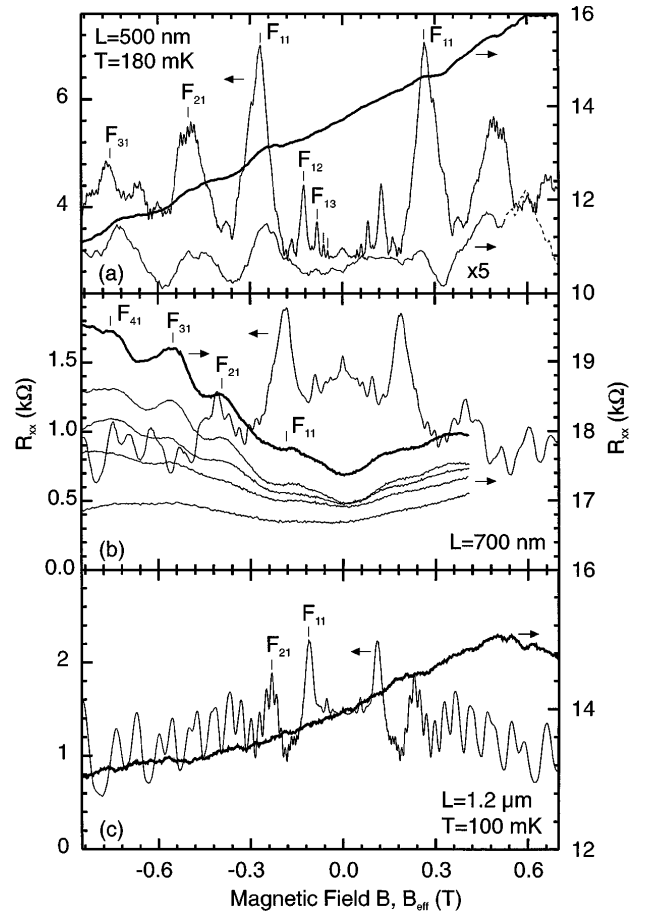


FIG. 3. Comparison of the electron (left axes) and CF (right axes) magnetic focusing spectra for  $L = 500 \text{ nm}$ ,  $700 \text{ nm}$ , and  $1.2 \mu\text{m}$  cavity arrays with respective carrier concentrations—after different levels of illumination—of  $1.4 \times 10^{11}$ ,  $2.0 \times 10^{11}$ , and  $1.55 \times 10^{11} \text{ cm}^{-2}$ . For ease of comparison, the magnetic field scale of the CF curves has been divided by  $\sqrt{2}$  and the curves have been shifted horizontally to make  $B_{1/2}$  coincide with  $B = 0$ . The CF traces in (a) and (b) show pronounced focusing peaks  $F_{ij}$  for negative (effective) field ( $\nu > 1/2$ ). For the  $L = 1.2 \mu\text{m}$  cavity they are absent. Only a weak  $F_{11}$  focusing peak can be discerned in (a) for positive effective field. The bottom curve in (a) has been obtained by subtracting a linear background from the CF curve ( $\times 5$ ,  $10 \text{ k}\Omega$  offset). CF curves in (b) do not go beyond  $B_{\text{eff}} = 0.5 \text{ T}$  since this corresponds to the maximum field of our magnet. For the CF traces in (b) the less pronounced asymmetry can be ascribed to a reduced saddle potential as expected for a larger  $n_s$  value. The temperature dependence of  $R_{xx}$  of the  $L = 700 \text{ nm}$  cavity array near  $\nu = 1/2$  has been indicated (from top to bottom: 100, 320, 700, 830 mK). Subsequent curves have a resistance offset of  $-200 \Omega$  for readability.

distinguish higher harmonics  $i$  is lost. Different from the dual-quantum-point-contact geometry [9], focusing peaks are observed for both positive and negative  $B$ , since each constriction simultaneously serves as injector and collector.

The  $R_{xx}$  traces around  $\nu = 1/2$  are also depicted in Fig. 3. Oscillatory structure, reproducible upon thermal cycling and absent in the unpatterned section, is clearly visible for the 500 and 700 nm period arrays, but has vanished for a cavity length  $L$  of  $1.2 \mu\text{m}$ . To establish that quasiclassical focusing of the CF is equivalent to its electron counterpart at weak magnetic fields, resistance maxima should be looked for at resonant effective magnetic field intervals that differ by a factor of  $\sqrt{2}$  from those determined from Eq. (1)—due to complete spin polarization at  $B_{1/2}$  [2]. Scaling the magnetic field axes of the high-field traces by  $1/\sqrt{2}$  results in a remarkable coincidence between the high- and low-field features and serves, together with the proper scaling behavior with cavity length, as compelling evidence that these features around  $\nu = 1/2$  can be attributed to transverse magnetic focusing of CFs. The focusing features are washed out upon raising the temperature above 700 mK [Fig. 3(b)], whereas electron-focusing peaks persist up to temperatures exceeding 20 K. Subharmonics ( $j > 1$ ), requiring ballistic transport across larger distances, are not resolved. Strikingly, more harmonics appear near  $\nu = 1/2$  than around  $B = 0$  [ $F_{31}$  and  $F_{41}$  in Fig. 3(b)]. Although an analysis of the amplitude of the focusing features is made difficult because of the background resistance, there appears to be no clear downward trend with increasing index  $i$ , in sharp contrast to the electron case. Finally, one notices a clearly developed asymmetry in  $R_{xx}$  around  $\nu = 1/2$  for the CF trace in Figs. 2 and 3(a). Although the fundamental focusing peak  $F_{11}$  shows up at either side, higher harmonics are weaker for  $B_{\text{eff}} > 0$  ( $\nu < 1/2$ ).

To gain a qualitative understanding of the observed differences between the focusing behavior of CFs and electrons, their quasiclassical dynamics has been studied. These differences are (i) the increasing (instead of decreasing) heights of the focusing peaks for increasingly negative  $B_{\text{eff}}^0$ , (ii) the asymmetry of the focusing peaks for positive and negative effective magnetic fields  $B_{\text{eff}}^0$ , and (iii) the larger magnetic field range over which focusing peaks are observed. In a hard-wall potential both the electron and CF dynamics would be identical. However, when using a model potential  $U(x, y)$  with *soft* walls, as in experiment, differences are anticipated, since changes in the density cause a spatially varying effective magnetic field for CFs according to [10]

$$B_{\text{eff}}(x, y) = B_{\text{eff}}^0 + B_{1/2} \frac{U(x, y)}{E_F}, \quad (2)$$

where  $E_F$  is the Fermi energy and  $B_{\text{eff}}^0 = B - B_{1/2}$  is the effective magnetic field far away from the *soft* walls.

Details of the calculations will be given elsewhere [11]. However, it is worth noting that the unknown mass of the CFs does not affect their trajectories even in arbitrary potentials, but only their velocities [10].

The use of a simple 3-constriction model with saddle-point potentials in each opening [Fig. 4(a)] allows one to understand the above-mentioned differences found in experiment. Electrons and CFs are ejected from the central emitter (out of the cavities in experiment) marked by an arrow. The reflection coefficient  $R$ , i.e., the probability for a trajectory to return through any of the 3 openings, is calculated assuming perfect specular reflection for electrons and CFs in Figs. 4(a) and 4(b), respectively. The fine structure of  $R_{xx}$  in the experiment is directly related to  $R$ . From the central opening two

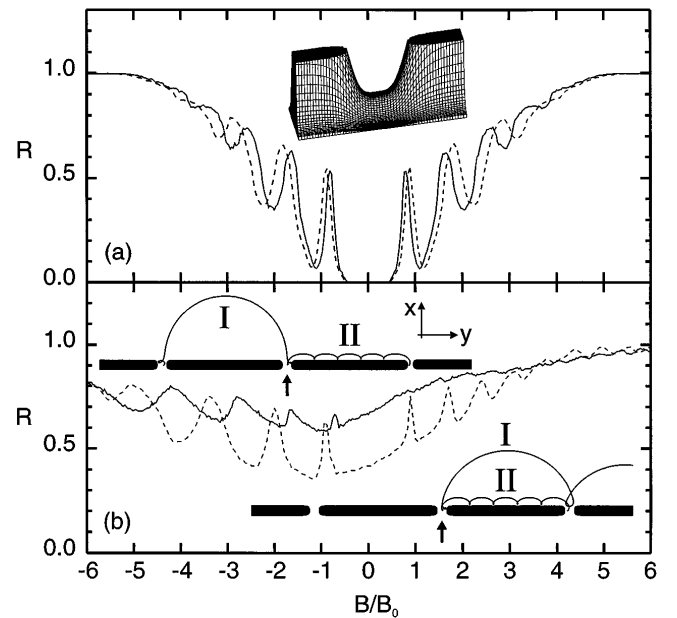


FIG. 4. The reflection coefficient  $R$  is shown for (a) electrons vs magnetic field and (b) CFs vs *effective* magnetic field in units of  $B_0$  corresponding to a cyclotron diameter  $L$  far from the constrictions. Particles are injected from the central opening, marked by an arrow, of the 3-constriction model potential  $U(x, y) = U_0 U_x(x) U_y(y - L) U_y(y) U_y(y + L)$  with  $U_x(x) = 1/([x/\Delta x]^\beta + 1)$ ,  $U_y(y) = 1 - U_1/([y/\Delta y]^\beta + 1)$ ,  $\beta = 4.0$ ,  $U_0 = 2E_F$ ,  $\Delta x = 0.04L$ , and  $\Delta y = 0.19L$  (see insets). The width of the potential wall and of the openings are controlled by, respectively,  $\Delta x$  and  $\Delta y$ , and  $U_1$  determines the saddle-point height. Without saddle points in the openings one finds only a very weak asymmetry for CFs between both field directions as suggested by the calculations for two different saddle-point heights:  $U_1 = 0.85$  (solid) and  $U_1 = 0.925$  (dashed). The insets in (b) show the different types of trajectories at  $|B_{\text{eff}}^0| \approx 2\hbar k_F/eL$  for positive (right) and negative (left) field directions. Both electron and CF traces show deviations from those corresponding to the focusing condition in Eq. (1): a downward shift of the peaks for electrons, associated with the reduction of the Fermi wave vector  $k_F^e$  in the soft-wall and saddle regions and a more complex behavior of peak position as well as a broadening for those of CFs reflecting the fact that, unlike electrons, CFs are not subject to a constant magnetic field, but rather to a range of field strengths.

different types of CF trajectories start [Fig. 4(b) insets]: type-I trajectories that descend into the flat region where they may contribute to the magnetic focusing and type-II trajectories that perform skipping motion near the potential wall due to the strong effective magnetic field [Eq. (2)].

For *positive*  $B_{\text{eff}}^0$ , the directions of motion for type-I and type-II trajectories are identical and equal to the direction of edge channels. The effective magnetic field is even enhanced in the saddle-point regions, the majority of the trajectories perform skipping motion along the walls (II) and only a few type-I orbits exist. Furthermore, the latter have only a small probability to cross the saddle point into the right-hand opening, because of the strong effective magnetic field in this area [see Fig. 4(b), the right inset]. As a result, the focusing peaks are weakened. For *negative* effective fields, the direction of motion of type-II orbits remains unchanged, whereas type-I orbits are deflected in the *opposite direction*.  $B_{\text{eff}}^0$  and  $B_{1/2}$  have opposite signs and the magnitude of  $B_{\text{eff}}(x, y)$  at the saddles decreases with decreasing  $B$  allowing more and more CF trajectories of type-I to leave the injector and to contribute to the focusing commensurability. In addition, it becomes easier for them to pass over the saddle in the left opening. These arguments account for the increasing size of the focusing peaks (i) and the asymmetry (ii).

For even more negative  $B_{\text{eff}}^0$ , the size of the CF focusing peaks will eventually decrease (as it does for electrons from the first harmonic) due to the decreasing ratio of cyclotron radius to constriction widths. For CFs, however, the opening widths are effectively reduced, because of the large phase-space volume occupied by type-II orbits that do not contribute to the focusing commensurability. For example, one finds for  $B_{\text{eff}}^0 = 0$  more than 40% type-II orbits, reducing the effective constriction widths by almost a factor of 2. This explains the larger field range over which focusing peaks are observed (iii).

Transverse magnetic focusing of CFs has previously been looked for by Goldman *et al.* [5] in the conventional dual quantum point contact (QPC) geometry [9]. Contrary to our experiment in which focusing disappears when the distance between neighboring cavities exceeds  $1 \mu\text{m}$ , *only* for QPC distances of several microns—1 order of magnitude larger than the expected CF mean free path—quasiperiodic fluctuations with a pronounced asymmetry in amplitude around half filling (large amplitude for  $B_{\text{eff}} > 0$ ) were measured and persisted up to 100 mK. When retaining the direction of the external magnetic field, but interchanging current and voltage contacts, CFs are expected to deflect in the direction opposite

to that of electrons. However, for this configuration the expected focusing signals for  $B_{\text{eff}} < 0$  were not observed [12]. Both the experimental data and the simulations in this work do not support this observation. In view of the large discrepancy between the CF mean free path and QPC distance, an alternative explanation of a fluctuating Fermi surface based on the quantum Boltzmann transport equation has been explored in Ref. [13]. Even in the magnetic field region corresponding to  $\nu < 1/2$  fluctuations appeared where they were not anticipated, and it was argued that those were reminiscent of universal conduction fluctuations [5]. The technique of ensemble averaging by arranging a large number of cavities on a single Hall bar was adopted in this work to effectively suppress conductance fluctuations and allow for the observation of the focusing peaks, which are in remarkable agreement with the “classical” CF dynamics in soft potentials.

We thank M. Riek, F. Schartner, B. Schönherr, and U. Waizmann for help in sample preparation and R. Haug for assistance with the dilution refrigerator. This work has been supported by the European Community Project “Human Capital and Mobility,” Physics in High Magnetic Fields, and the Deutsche Forschungsgemeinschaft.

- 
- [1] J. K. Jain, Phys. Rev. Lett. **63**, 199 (1989).
  - [2] B. I. Halperin, P. A. Lee, and N. Read, Phys. Rev. B **47**, 7312 (1993).
  - [3] W. Kang, H. L. Störmer, and L. N. Pfeiffer, Phys. Rev. Lett. **71**, 3850 (1993).
  - [4] R. L. Willet, R. R. Ruel, K. W. West, and L. N. Pfeiffer, Phys. Rev. Lett. **71**, 3846 (1993).
  - [5] V. J. Goldman, B. Su, and J. K. Jain, Phys. Rev. Lett. **72**, 2065 (1994).
  - [6] G. Lütjering *et al.*, in Proceedings of the 11th International Conference on the Electronic Properties of Two Dimensional Systems, 1995 [Surf. Sci. (to be published)].
  - [7] K. Nakamura *et al.*, Appl. Phys. Lett. **56**, 385 (1990).
  - [8] A. M. Chang, H. U. Baranger, L. N. Pfeiffer, and K. W. West, Phys. Rev. Lett. **73**, 2111 (1994).
  - [9] H. van Houten *et al.*, Phys. Rev. B **39**, 8556 (1989).
  - [10] R. Fleischmann, T. Geisel, C. Holzknicht, and R. Ketzmerick, www site <http://xxx.lanl.gov/abs/cond-mat/9509168>.
  - [11] R. Fleischmann, T. Geisel, and R. Ketzmerick (to be published).
  - [12] J. K. Jain and V. J. Goldman (private communication).
  - [13] Y. B. Kim, P. A. Lee, and X.-G. Wen, www site <http://xxx.lanl.gov/abs/cond-mat/9504063>.
  - [14] I. V. Kukushkin, R. J. Haug, K. von Klitzing, and K. Eberl, Phys. Rev. B **51**, R18045 (1995).